



# Fluorescent cellulose nanocrystals for the detection of lead ions in complete aqueous solution

Ruyuan Song · Qing Zhang · Youlu Chu · Lei Zhang · Hongqi Dai · Weibing Wu

Received: 21 May 2019 / Accepted: 17 September 2019 / Published online: 30 September 2019  
© Springer Nature B.V. 2019

**Abstract** A fluorescent probe for the detection of lead ions in complete aqueous solution was synthesized by covalently combining a fluorescent 1,8-naphthalimide dye with cellulose nanocrystals (CNCs). The dye-labelled CNCs have lots of carboxyl and hydroxyl groups on the surface, which make them disperse well in water. There is little fluorescence discrimination for 1,8-naphthalimide dye in the presence of different metal ions, while the fluorescent CNCs exhibit selective and sensitive response to Pb(II) with remarkably enhanced emission intensity.

The limit of detection of the fluorescent CNCs is as low as  $1.5 \times 10^{-7}$  mol/L, and there is good linear relationship between the fluorescence maxima and the Pb(II) concentration in a wide range of  $2.5 \times 10^{-7}$ – $5.0 \times 10^{-5}$  mol/L. The sensing ability of the dye-labeled CNCs to Pb(II) is ascribed to the synergistic complexation of Pb(II) with both the grafted dye groups and the adjacent carboxyl groups on the surface of the CNCs. The combination ratio of Pb(II) to the fluorophore on CNCs is determined to be 1.2:1 via Job's plot experiment, which is basically consistent with the theoretical value of 1:1. The offered fluorescent CNCs can be employed as a nanosensor for the detection of metal ions and can be further promoted for many applications in chemical, environmental, and biological systems.

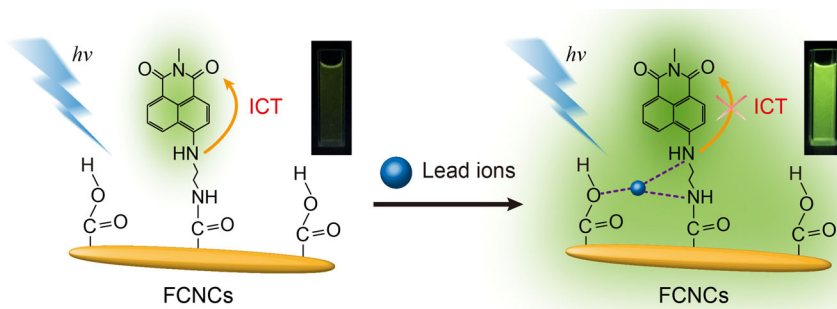
**Electronic supplementary material** The online version of this article (<https://doi.org/10.1007/s10570-019-02760-y>) contains supplementary material, which is available to authorized users.

R. Song · Q. Zhang · Y. Chu · H. Dai · W. Wu (✉)  
Jiangsu Co-Innovation Center for Efficient Processing and Utilization of Forest Resources, Jiangsu Provincial Key Lab of Pulp and Paper Science and Technology, Nanjing Forestry University, Nanjing 210037, China  
e-mail: wbwu@njfu.edu.cn

L. Zhang (✉)  
Key Laboratory for Organic Electronics and Information, National Jiangsu Synergetic Innovation Center for Advanced Materials (SICAM), Nanjing University of Posts and Telecommunications, Nanjing 210023, China  
e-mail: iamlzhang@njupt.edu.cn

W. Wu  
State Key Laboratory of Biobased Material and Green Papermaking, Qilu University of Technology, Shandong Academy of Sciences, Jinan 250353, China

**Graphic abstract** Water-dispersible fluorescent probe via covalent immobilization of 1,8-naphthalimide on cellulose nanocrystals (CNCs) exhibits selective and sensitive detection of lead ions in complete aqueous solution. The inhibited intramolecular charge transfer process (ICT) of the fluorophores loaded on CNCs contributes to the remarkably enhanced fluorescence emission in the presence of lead ions.



**Keywords** Cellulose nanocrystals · Fluorescent probe · Metal ion · Intramolecular charge transfer

## Introduction

In recent decades, a variety of fluorescent probes have been prepared and their potential application has been demonstrated in many areas, such as metal ion detection, biological imaging, cell labeling, and etc., due to the good selectivity, high sensitivity, high response speed and simple operation (Wang et al. 2019; Salarvand et al. 2019). Organic dyes are widely used for fluorescent probes because of their diversity and modifiability (Chen et al. 2011, 2019). However, most of the organic dyes are hydrophobic and have the shortages of poor water-solubility and biocompatibility (Shaki et al. 2010). An effective solution is covalently coupling organic dyes to hydrophilic and biocompatible nanocarriers, such as silica nanoparticles (Xia et al. 2014; Xie et al. 2014; Zhang and Yu 2014), metal nanoparticles (Liu et al. 2013; Makwana et al. 2015) and polymer nanoparticles (Suárez et al. 2018; Jiang et al. 2018; Fu et al. 2018). The dye-labeled nanocomposites combine the advantages of organic dyes and nanocarriers, making them ideal fluorescent probes for the sensitive, selective, low-cost and facile detection of different analytes (Amirjani

and Haghshenas 2018). Wu et al. grafted fluorescent dye onto the surface of the mesoporous silica nanoparticles to prepare a water-soluble fluorescent sensor for the selective detection and removal of Ag(I) in aqueous solutions (Wu et al. 2018a). Wang et al. developed a stable fluorescent probe by immobilizing the near-infrared (NIR) brilliant cresyl blue (BCB) on gold nanoparticle (AuNPs), which could detect Pb(II) ions with less interference and high sensitivity in aqueous solution (Wang et al. 2015).

Cellulose nanocrystals (CNCs), which are obtained by the acid hydrolysis of the amorphous regions in native cellulose, are rod-like particles with size of 50–300 nm in length and 3–20 nm in width (Golmohammadi et al. 2017). CNCs possess the advantages of high strength, large specific surface area, renewability, hydrophilicity, biodegradability and biocompatibility. Because of the existence of active groups on the surface, CNCs are also good template carriers for the multifunctional modification (Wu et al. 2015; Wu et al. 2018b). Fluorescent probes via the dye decoration of CNCs combine the advantages of both organic dye and CNC carrier, and much research has been done on the synthesis and application of dye-labeled CNCs (Zhang et al. 2018). Ding et al. attached Rhodamine B isothiocyanate (RBITC) to CNCs with high labeling efficiency by means of electrostatic adsorption and covalent bonding. Compared to the free dye, the fluorescent CNCs have higher quantum

yield and longer fluorescence lifetime (Ding et al. 2017). Pyrene-labeled CNCs by a three-step procedure have been reported to exhibit high selectivity towards Fe(III) among other screened metal ions and show good discrimination between Fe(II) and Fe(III) (Zhang et al. 2012). Rhodamine spiroamide groups were also covalently immobilized onto CNCs to fabricate fluorescent nanocomposites with multiple responsiveness to pH-values, heat and UV light. The fluorescence change induced by external stimuli refers to a ring opening and closing process of the linked rhodamine spiroamide groups (Zhao et al. 2014).

1,8-naphthalimide is a fluorophore with a large conjugated system and coplanarity (Duke et al. 2010). When an electron donating group is introduced into the 4 position of the 1,8-naphthalimide, a typical D- $\pi$ -A structure is formed. The electrons are easily excited by light, resulting in the fluorescence emission (Nandhikonda et al. 2009). Because of their unique structure, 1,8-naphthalimide dyes have photostability, high quantum yield, and photoresponsiveness, providing an excellent sensing mode for the development of sensors and probes (Loving and Imperiali 2009; Bojinov and Konstantinova 2007). In this study, we developed a fluorescent probe with sensitive and selective fluorescence response to Pb(II) by the covalent immobilization of 1,8-naphthalimide dye on CNC substrate. The sensing performance and mechanism of the dye-labeled CNCs to metal ions were thoroughly investigated. The synergistic effect of CNC substrate not only provides good water dispersion stability, but also greatly enhances the fluorescent sensitivity and selectivity of 1,8-naphthalimide fluorophores to Pb(II) in aqueous solutions.

## Experimental

### Chemicals

(2,2,6,6-Tetramethyl-piperidin-1-yl)-oxyl (TEMPO) (98%) were purchased from Sigma-Aldrich. Sodium hypochlorite (NaClO), sodium bromide (NaBr), sodium hydroxide (NaOH), hydrochloric acid (HCl), sodium thiosulfate (Na<sub>2</sub>S<sub>2</sub>O<sub>3</sub>), sodium chloride (NaCl), sodium nitrate (NaNO<sub>3</sub>), sodium sulphate (Na<sub>2</sub>SO<sub>4</sub>), silver nitrate (AgNO<sub>3</sub>), lead nitrate (Pb(NO<sub>3</sub>)<sub>2</sub>), copper nitrate trihydrate (Cu(NO<sub>3</sub>)<sub>2</sub>·3H<sub>2</sub>O), zinc chloride (ZnCl<sub>2</sub>), magnesium nitrate

hexahydrate (Mg(NO<sub>3</sub>)<sub>2</sub>·6H<sub>2</sub>O), ferrous chloride tetrahydrate (FeCl<sub>2</sub>·4H<sub>2</sub>O), barium chloride (BaCl<sub>2</sub>), cobalt chloride (CoCl<sub>2</sub>), copper sulfate (CuSO<sub>4</sub>), nickel sulfate hexahydrate (NiSO<sub>4</sub>·6H<sub>2</sub>O) and potassium dichromate (K<sub>2</sub>Cr<sub>2</sub>O<sub>4</sub>) were acquired from Nanjing Chemical Reagent Co., Ltd. 2-Methoxyethanol, ethanol, trichloromethane, triethylamine, methanamine, N,N-dimethylformamide were purchased from Sinopharm Chemical Reagent Co., Ltd. 4-Bromo-1,8-naphthalic anhydride was obtained from Zhengzhou Alpha Chemical Co., Ltd. Anhydrous ethylenediamine, 1-ethyl-3-(3-dimethylaminopropyl) carbodiimide (EDC), N-hydroxysuccinimide (NHS) were acquired from TCI (Shanghai) Co., Ltd. The deionized water was made by a Ulupure purification system (UPT-II-20T, resistivity higher than 18 M $\Omega^3$  cm<sup>-1</sup>).

### Preparation of nanofibrillated cellulose (NFC)

Bleached soft wood pulp (12 g) was soaked in deionized water (1 L), stirred and dismantled with a power basic stirrer. TEMPO (0.192 g), NaBr (1.92 g) and NaClO (6.6 wt%, 132 mL) were added in the suspension and the pH was adjusted between 10 and 10.5 with 0.2 mol/L NaOH (Benhamou et al. 2014). The mixture was stirred for 4 h until the pH was not changed (Fukuzumi et al. 2013). The resulting pulp was soaked in HCl solution (0.1 mol/L, 1000 mL) and then purified with deionized water by filtration. Finally, the product was ultrasonicated at consistency of 1 wt% for 5 min. The samples were freeze-dried for 3 days at -98 °C and 20 Pa after pre-freezing at -20 °C for 12 h.

### Preparation of carboxylated cellulose nanocrystals (CCNCs)

The freeze-dried NFC (3.77 g) and HCl (3 mol/L, 200 mL) were placed in a flask (500 mL) equipped with condenser, and the suspension was refluxed for 3 h. The sample was washed with deionized water by centrifugation at a high speed (10,000 rpm, 10 min) for several times until the supernatant was no longer clear and transparent. Finally, the suspension of CCNCs was dialyzed against distilled water until neutral (Zhou et al. 2015).

## Synthesis of fluorescent dye and fluorescent cellulose nanocrystals (FCNCs)

Fluorescent dye of 4-((2-aminoethyl)amino)-9-methyl-1,8-naphthalimide (AANI) is synthesized according to previous literatures (Grabtchev et al. 1997; John 1990). Details can be found in the supporting information. The preparation of fluorescent cellulose nanocrystals (FCNCs) is as follows: First, the aqueous suspension of CCNCs (2 mg/mL, 200 mL) was sonicated for 15 min. Then EDC (550 mg, 2.87 mmol) was added and the pH was maintained at 5.2 for 30 min. Subsequently, NHS (65.98 mg, 0.57 mmol) was added and the pH was adjusted to 7.2 with PBS buffer. Afterwards, the solution of AANI (25 mg, 0.093 mmol) in DMF (5 mL) was added to above suspension. The mixture was stirred for 16 h in the dark at room temperature. After reaction, the product was purified by multiple centrifugal washing (10,000 rpm, 10 min) with deionized water and dialysis with distilled water until the dialyzate was clear and transparent (Zhou et al. 2015).

## Characterization and detection

The FTIR spectra were collected at 4000–650  $\text{cm}^{-1}$  wavelength range using Fourier transform infrared spectrometer (FTIR-650, Tianjin Gangdong Co., Ltd.) equipped with single attenuated total reflectance system. Measurements were performed by accumulating 32 scans with a spectral resolution of 2  $\text{cm}^{-1}$ . The images of Atomic force microscopic (AFM) were obtained using a Atomic Force Microscope (Dimesion Edge, Bruker Co.) at the frequency of 1.0 Hz. The samples for the CCNCs and FCNCs suspensions (0.001 wt%) were deposited from aqueous solution on silicon wafers and dried at 40 °C. The scan range was 5  $\mu\text{m}$ .

Nuclear magnetic resonance (NMR) experiments were performed using a Advance III HD all-digital NMR spectrometer (400 MHz, Bruker Co., Ltd.). Solid-state NMR (ssNMR) experiments were performed on Bruker Avance III (proton radio frequency of 400 MHz) with a double resonance HX probe. The method of the detection was cross-polarization-magic angle spinning (CP/MAS). The ssNMR was operated at a magic angle spinning (MAS) rate of 10 kHz with the contact time of 2 ms. The proton dipolar decoupling was achieved by applying two-pulse phase

modulation (TPPM15) on the  $^1\text{H}$  channel during acquisition (Chang et al. 2016). The excitation pulse length was 5  $\mu\text{s}$  for  $^{13}\text{C}$  and the repetition delay was 4 s.

XPS experiments were performed in a X-ray photoelectron spectrometer (AXIS UltraDLD, Shimadzu). Survey spectra were collected from 1200 to 0 eV at a pass energy of 160 eV with a scan step of 1.0 eV. High resolution spectra of C1s, O1s and N1s were recorded at a pass energy of 40 eV with a scan step of 0.1 eV. Powder samples adhered on conductive tape were used for the measurement. Monochromation Al K $\alpha$  (1486.6 eV) was used as the excitation source. The charge neutralization was performed using charge neutralizer gun. The resulting spectra charge were referenced to the C1s line at 284.8 eV from adventitious carbon. The relative sensitivity factors (RSF) of C1s, O1s and N1s for quantification were 0.278, 0.78 and 0.477, respectively. Background type of line was used for integration.

Elemental analysis (EA) for the elements of C, H and N was carried out on an Organic Elemental Analyzer (PE2400II). with the accuracy of analysis less than 0.03%. About 5 mg of CCNCs and FCNCs were encapsulated in tinfoil for combustion.

## General fluorescence measurements

Fluorescence spectra were measured by Fibre-Optical Spectrometer equipped with fp-405-T01-FL Laser (R4, Shanghai Ideaoptics Co., Ltd.). The excitation wavelength and the slit width were set at 405 nm and 2 nm, respectively. To compare the fluorescent behaviors between AANI and FCNCs, the initial fluorescent intensity of FCNCs suspension was set to be the same as that of AANI solution without the addition of metal ions. In this experiment, the testing concentrations of FCNCs suspension and AANI solution were 0.01 wt% and  $2.86 \times 10^{-6}$  mol/L, respectively. All fluorescence measurements were carried out in distilled water at pH 6.8. Emission spectra of FCNCs in the presence of various metal ions (Na(I), Mg(II), Fe(II), Ni(II), Co(II), Cu(II), Zn(II), Ag(I), Ba(II) and Pb(II)) were measured.

## Determination of detection limit

The detection limit of FCNCs for Pb(II) was calculated by using the emission titration data. The emission spectrum of FCNCs without Pb(II) was measured 10 times to achieve the standard deviation of blank measurement. The slope of the line was obtained by plotting the intensities of FCNCs at 540 nm against concentration of Pb(II) and each emission intensity was measured for three times. The following equation was used to calculate the limit of detection (LOD) (Rasheed et al. 2019; Neupane et al. 2016).

$$\text{LOD} = 3\sigma/m \quad (1)$$

where  $\sigma$  is the standard deviation of the emission intensity of the blank FCNCs, and  $m$  is the slope between the emission intensity vs. concentration.

## Results and discussion

### Morphology and structure of FCNCs

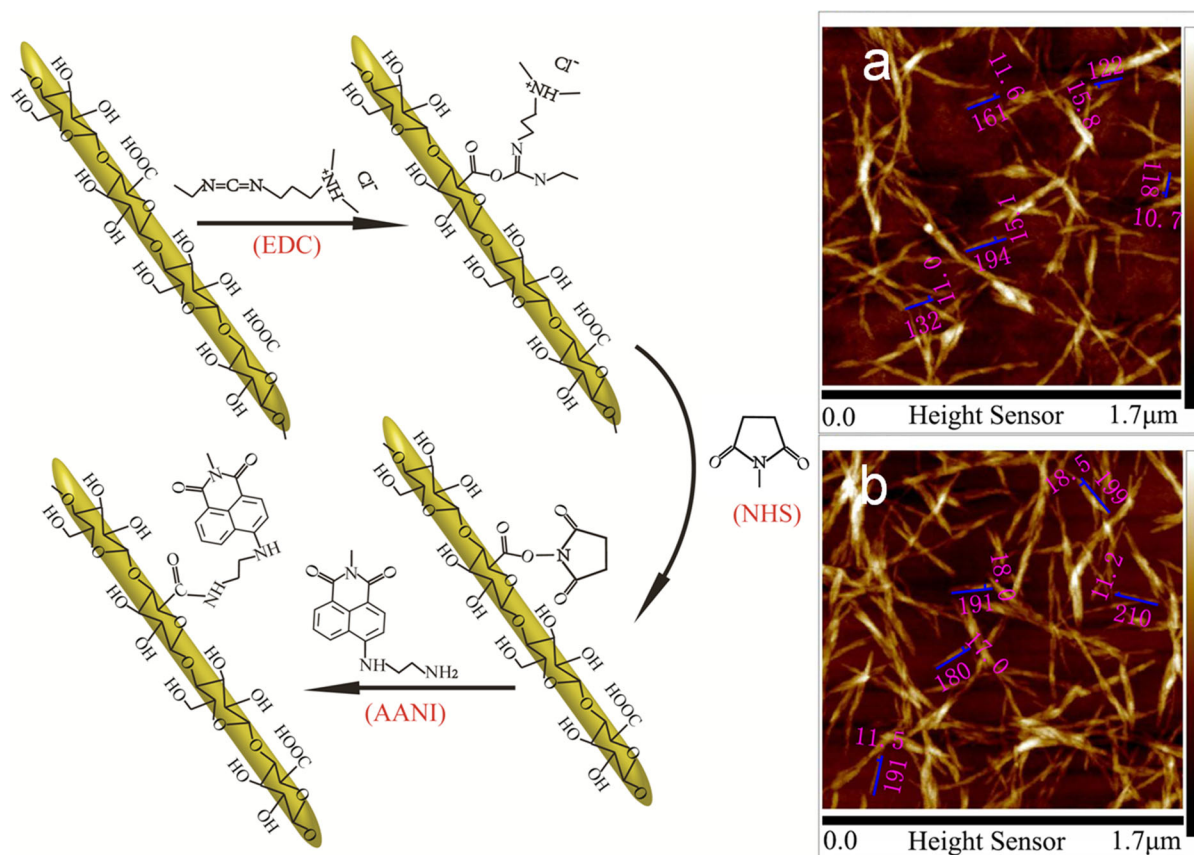
CCNCs with 10–18 nm in width and 100–250 nm in length were obtained via TEMPO-mediated oxidation and HCl hydrolysis (Fig. 1a). The carboxyl content of CCNCs was determined to be 1.52 mmol/g via conductive titration (Fig. S2) (Chen et al. 2017). AANI was covalently immobilized on the surface of CCNCs via the EDC/NHS-mediated reaction between carboxyl and the amino groups, leading to dye-labeled FCNCs, as shown in Fig. 1. During the reaction process, EDC with strong chemical reactivity first reacted with carboxyl group to form an active intermediate (Powell and Boyce 2006). NHS subsequently stabilized the intermediate by avoiding the hydrolysis which could easily occur when EDC was used alone in aqueous solution (Sam et al. 2009; Ward et al. 2017). EDC/NHS are non-toxic and biocompatible cross-linking agents, which can be converted into water-soluble derivatives during the reaction and do not exist in the final product (Ghassemi and Slaughter 2018). After EDC/NHS-mediated coupling, FCNCs maintain the rod-like morphology and the dimensions are comparable to those of original CCNCs as evidenced by AFM (Fig. 1b) (Eisa et al. 2018). The successful dye attachment of FCNCs was confirmed by the reduced stretch absorption at  $1729\text{ cm}^{-1}$  of

carboxyl and increased absorption band at  $1678\text{ cm}^{-1}$  of amide, as shown in Fig. 2.

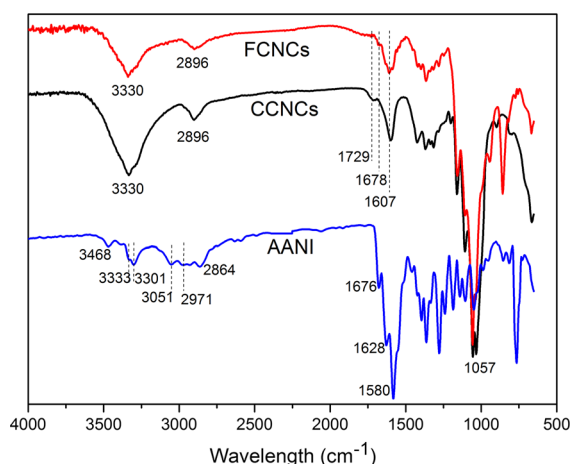
The immobilization of AANI on the surface of CCNCs was further verified by XPS. The XPS spectra obtained for CCNCs and FCNCs are shown in Fig. 3. The spectrum of CCNCs exhibits the presence of two peaks at around 286 and 531 eV, which correspond to C1s and O1s, respectively. For FCNCs, a new peak appears at approximately 402 eV, indicating the successful amidation reaction of carboxyl groups on the surface (Chen et al. 2017; Tang et al. 2016). High resolution spectra of C1s peaks reveal the functional composition of the carbon and oxygen species for CCNCs and FCNCs (Fig. 3b, d). Detailed peak fitting data are listed in Table S1. Compared with CCNCs, the increased atomic concentrations of C–C and O–C=O/N–C=O signal can be ascribed to the introduction of naphthalene ring and amide groups on the surface of FCNCs. The peak-differentiation-imitating analysis of O1s high resolution spectra also provides the evidence of covalent immobilization of AANI on CCNCs (Fig. S2). There is a new deconvoluted peak at 530.93 eV for FCNCs, which can be ascribed to the formation of amide and the introduction of imide on the surface of FCNCs. The elemental composition by XPS analysis shows an obvious increases in the percentage of carbon and nitrogen atoms from CCNCs to FCNCs, which is consistent with the conclusion from C1s and O1s high resolution spectra (Table S2). In addition, EA was employed to determine the dye content of FCNCs (Table S3). Based on the presence of 1.85% nitrogen, the content of immobilized fluorophore on FCNCs was determined to be 0.44 mmol/g according to Equation S1 and S2.

Figure 4 illustrates the  $^{13}\text{C}$  NMR spectra of CCNCs and FCNCs. For CCNCs, the broad peak around 104.1 ppm is assigned to anhydroglucose carbon C1. The resonance peaks at 70–80 ppm correspond to C2, C3, and C5, and the resonances for C4 appear at 83.3 and 87.7 ppm. The peaks at 61.5 and 64.1 ppm are associated with C6, the primary alcohol group of the anhydroglucose units. The upfield shoulder peaks for the C4 at 83.3 ppm and C6 at 61.5 ppm are attributed to the amorphous and surface regions of CNCs (Navarro et al. 2015). There are new peaks observed for FCNCs compared with CCNCs in the regions of 170–110 ppm and 50–20 ppm. The region of 170–110 ppm is further magnified and compared with





**Fig. 1** Schematic synthesis route of the covalent immobilization of 1,8-naphthalimide dye on the surface of CNC. The inserted pictures are the AFM images of CCNCs (a) and FCNCs (b)



**Fig. 2** FTIR spectra of AANI, CCNCs and FCNCs

the spectrum of AANI. It is noted that FCNCs and AANI have extremely similar spectral characteristics of the naphthalene ring (C3'–C12'). The signal peaks

at 25.5 and 38 ppm are related to C13', C14' and C16', which are the saturated carbons of the immobilized AANI. The signal peaks of amide (C15') may overlap with that of imide (C1', C2') at 165 ppm. The peak at 174 ppm corresponds to the remained carboxyl groups on the nanocrystal surface. Considering that FCNCs have been thoroughly purified to remove physically-adsorbed fluorophores, the presence of signals corresponding to those of AANI and CCNCs provides the evidence of covalent attachment for FCNCs.

#### Fluorescence response to metal ions

As mentioned above, the poor water solubility and dispersibility usually limit the application of organic dyes as fluorescent probes in 100% aqueous solution. Immobilization of fluorophore on hydrophilic substrate is a feasible way to fabricate water-dispersible fluorescent probe. FCNCs labeled with AANI possess

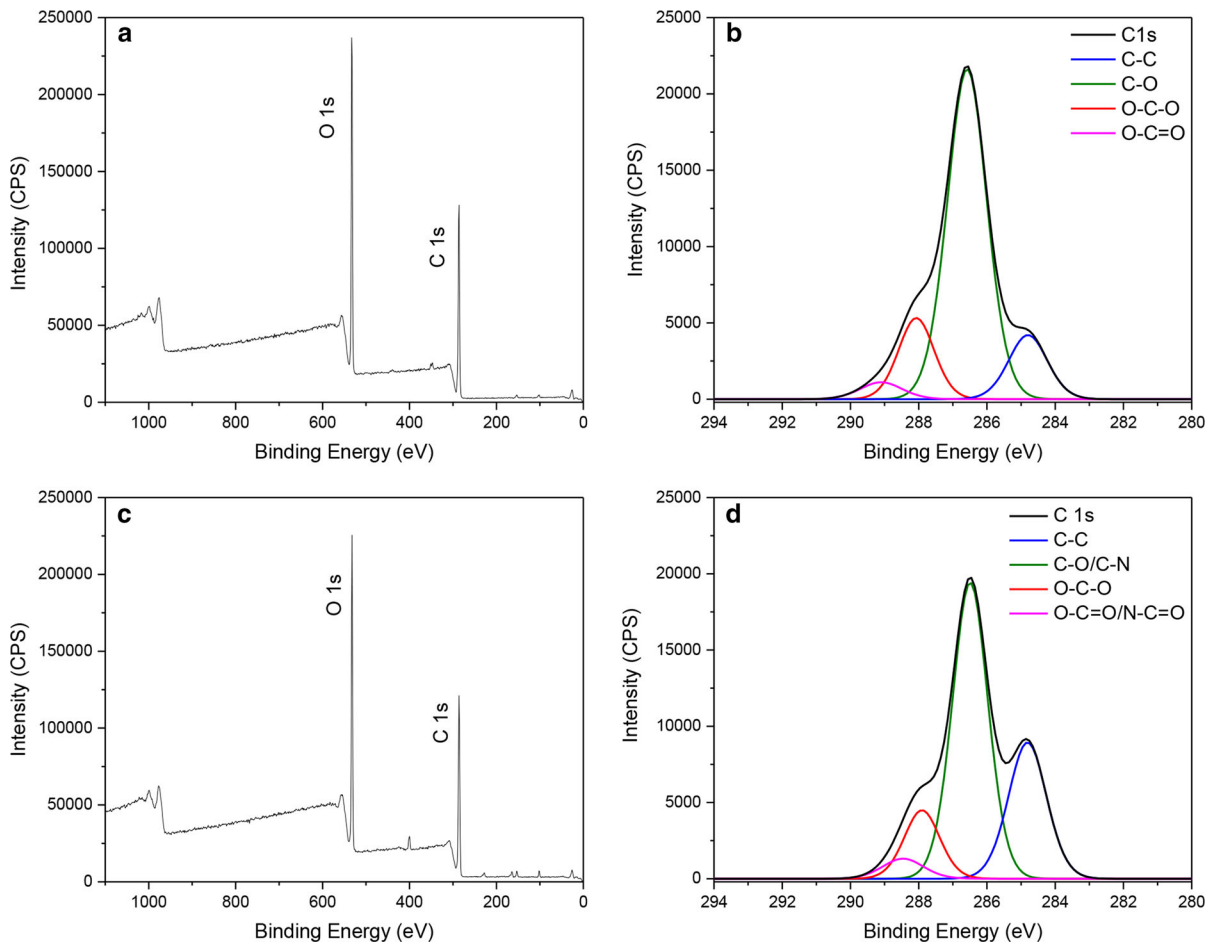


**Fig. 3** XPS survey spectra of CCNCs (a, b) and FCNCs (c, d). b and d high resolution spectra of the C1s peak

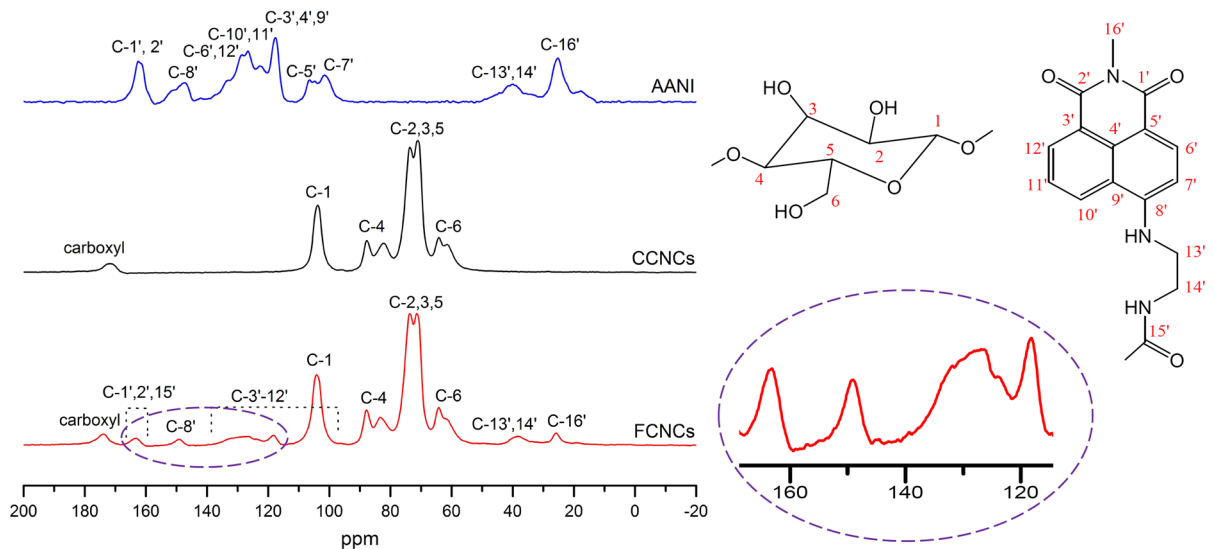


**Fig. 4** Solid  $^{13}\text{C}$  NMR spectra of AANI, CCNCs and FCNCs

good water dispersivity because of the presence of a large number of carboxyl and hydroxyl groups on the surface. The fluorescent behaviors of AANI and FCNCs were investigated in the aqueous solutions of metal ions ( $1.0 \times 10^{-4}$  mol/L) including Na(I), Mg(II), Fe(II), Ni(II), Co(II), Cu(II), Zn(II), Ag(I), Ba(II) and Pb(II), and the maximum emission intensities were recorded. There is no fluorescent responsiveness of AANI to metal ions, as shown in Fig. 5a. On the contrary, FCNCs show fluorescent sensitivity to different metal ions (Fig. 5b). Among the selected metal ions, Na(I) and Ag(I) have no significant impact on the fluorescent behavior of FCNCs. Divalent metal ions including Mg(II), Ba(II), Cu(II), Zn(II), Fe(II), Co(II), and Ni(II) show weak enhancement effects on the fluorescent intensity. It is worth noting that only Pb(II) significantly strengthens the fluorescence emission and the enhancement index (FE) is high up to 9.5. Figure 4c, d show the fluorescence spectra of AANI

and FCNCs with different metal ions in aqueous solution. The difference in the maximum emission wavelength ( $\lambda_{\max}$ ) was also observed besides the fluorescent intensity. With the addition of Na(I), Ag(I), Mg(II), Ni(II), Co(II), Fe(II), Zn(II), Cu(II), Ba(II) and Pb(II), the  $\lambda_{\max}$  of FCNCs shifts from 547.0 to 546.0, 545.6, 544.3, 543.6, 542.7, 542.3, 541.7, 541.5, 541.1 and 540.5 nm, respectively. It is noted that the  $\lambda_{\max}$  of FCNCs is gradually blue-shifted as the fluorescent intensity increases. The maximum blue shift for FCNCs in Pb(II) is about 6.5 nm compared to blank FCNCs. Obviously, the fluorescent responsiveness of FCNCs to metal ions is related to the CNC substrate compared with pure AANI. The special fluorescent behaviors in the presence of metal ions, especially Pb(II), could be ascribed to the complexation between metal ions, dye groups and CNC substrate.

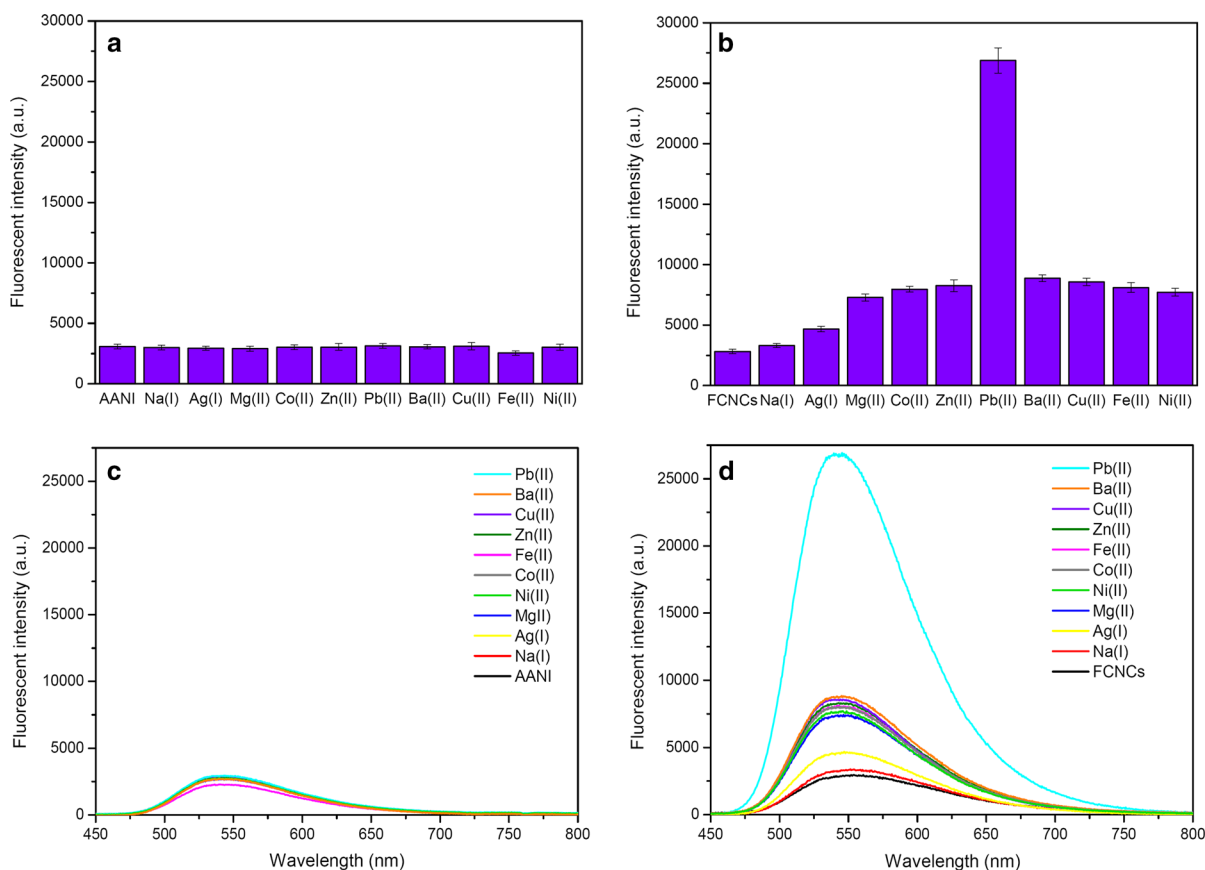


**Fig. 5** The fluorescence maxima of AANI (a), FCNCs (b) and the fluorescence emission spectra of AANI (c), FCNCs (d) in aqueous solution with different metal ions ( $1 \times 10^{-4}$  mol/L). AANI:  $2.86 \times 10^{-6}$  mol/L, FCNCs: 0.01 wt%. Excitation wavelength: 405 nm



To investigate the interference of coexistent metal ions on the fluorescent detection ability of FCNCs, the fluorescence maxima of FCNCs to Pb(II) were recorded under the co-existence of other screened metal ions. As shown in Fig. 6, the interfering metal ions show negligible or slight disturbance for the Pb(II)-dependent fluorescence response of FCNCs. The fluctuations of fluorescent intensity may be ascribed to the competitive interactions between metal ions and the change of environmental conditions. All the enhancement and attenuation effects are very slight, suggesting that FCNCs have relatively good anti-interference ability for detecting Pb(II). The influence of counter ions on fluorescent detection was also investigated using NaCl, NaBr, NaNO<sub>3</sub>, and Na<sub>2</sub>SO<sub>4</sub>. Different counter ions of Cl<sup>-</sup>, Br<sup>-</sup>, SO<sub>4</sub><sup>2-</sup> and NO<sub>3</sub><sup>-</sup> show no significant effect on the fluorescent behavior of FCNCs (Fig. S3).

The fluorescent behaviors of FCNCs with increasing concentration of Pb(II) were determined in 100% aqueous solutions. Figure 7a presents the fluorescence spectra of FCNCs in different Pb(II) concentrations. The fluorescence maximum of FCNCs quickly increases as the concentration of Pb(II) increases in the range of  $2.5 \times 10^{-6}$ – $1.0 \times 10^4$  mol/L and the trend slows down when the concentration is higher than  $1.0 \times 10^{-4}$  mol/L (Fig. 7b). The fluorescence maxima and the corresponding Pb(II) concentrations are selectively fitted linearly in the ranges of  $2.5 \times 10^{-7}$ – $5.0 \times 10^{-5}$  mol/L (Fig. 7c) and  $2.5 \times 10^{-7}$ – $1.0 \times 10^{-5}$  mol/L (Fig. 7d), respectively. The slopes of the two fitting lines are close, and both the

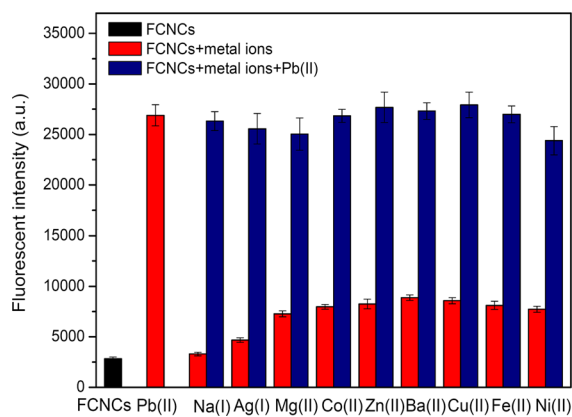


**Fig. 6** Effects of coexisting ions on the fluorescence maxima of the aqueous solution of FCNCs and Pb(II). FCNCs: 0.01 wt%, Pb(II):  $1.0 \times 10^{-4}$  mol/L

calculated values of  $R^2$  are higher than 0.999, indicating that the good linear relationship between the fluorescence maximum and the corresponding Pb(II) concentration in a wide concentration range. The detection sensitivity of FCNCs to Pb(II) in aqueous solution is determined on the basis of the fluorescence titration. The LOD of FCNCs is calculated to be  $1.5 \times 10^{-7}$  mol/L according to Eq. (1). The good selectivity, high sensitivity and liner relationship of response make FCNCs potential fluorescent probe to quantitatively detect trace levels of Pb(II) in 100% aqueous solutions.

#### Sensing mechanism of FCNCs for Pb(II)

Upon irradiating dyes with D- $\pi$ -A structure, intramolecular charge transfer (ICT) could occur and result in lower and more stable excited state accompanied by energy loss (Slama-Schwok et al. 1990). ICT is greatly affected by the polarity of the solvent. In solvents with high polarity, such as alcohol and water, the process of ICT is remarkably strengthened, causing a decrease in the fluorescent intensity and redshift in the maximum emission wavelength. These changes are attributed to the large non-radiative deactivation constants of the excited state in polar and protic solvents (Martin et al. 1996). For AANI, ITC specially refers to the charge transfer from the lone pair electrons of amine at one end to the imide at the other end through conjugated naphthalene ring after irradiation (Chatterjee et al. 2007). Decrease in the fluorescent intensity and redshift in the maximum emission wavelength with an increase in the solvent polarity were observed (Fig. S4), which is consistent with theoretical expectations. As discussed above, the fluorescence of AANI is little affected by the addition of metal ions, suggesting that there is no complexation between AANI and metal ions. However, the fluorescence behaviors of FCNCs are greatly different in the presence of metal ions. Three phenomena were observed including little effect on the fluorescence for univalent ions, slight increase in the fluorescent intensity for common divalent ions and remarkable emission enhancement for Pb(II). Based on the high binding ability of divalent metal ions with carboxyl groups, we believe that divalent metal ions can chelate with amine and amide of FCNCs to varying extent under the synergistic effect of carboxyl groups on the surface of CNC substrate. Therefore, the ICT process

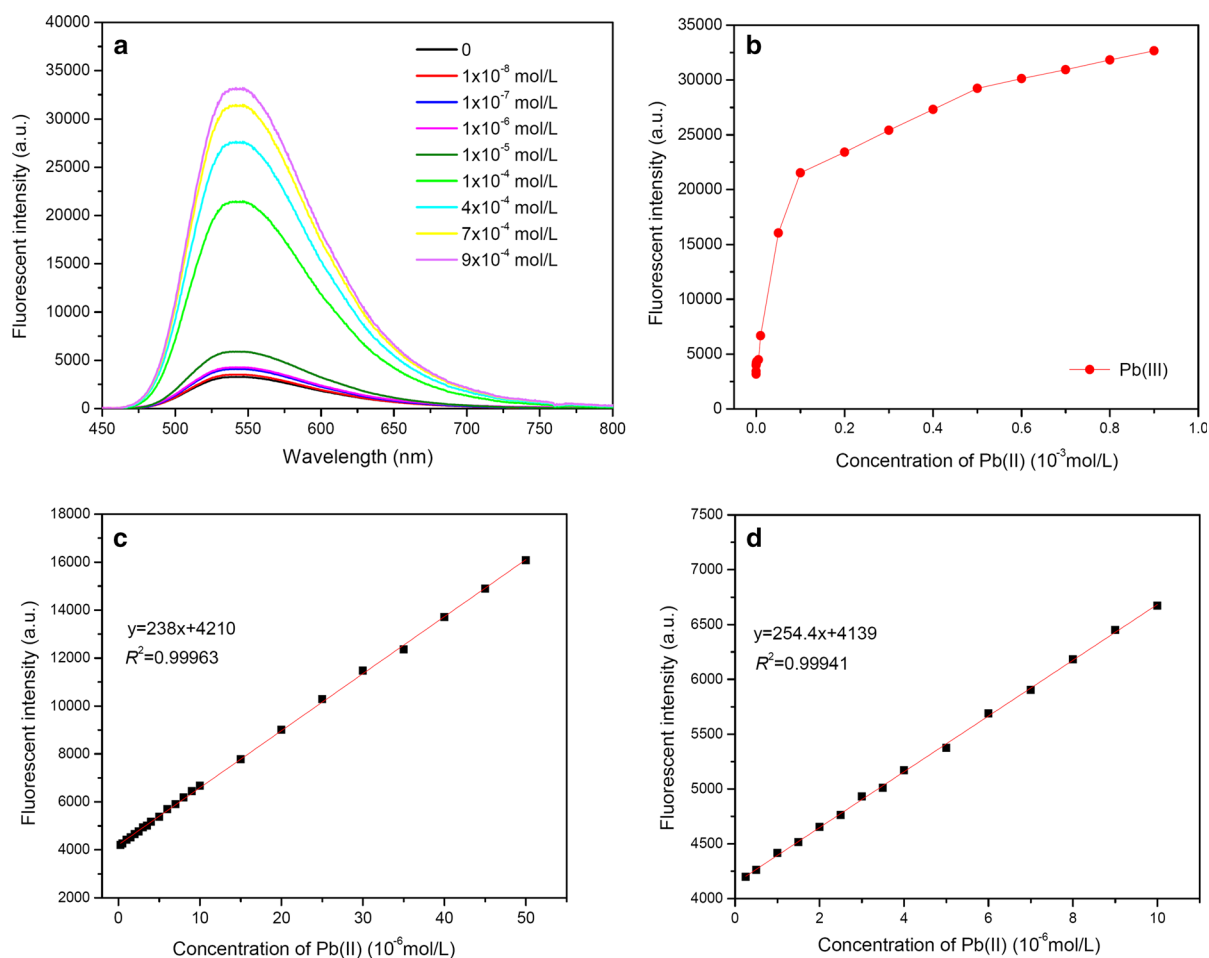


**Fig. 7** The fluorescence emission spectra of the FCNCs (0.01 wt%) for the detection of Pb(II) (a). Plot of fluorescence maxima with different concentrations of Pb(II) (b). Linear

change of fluorescence maxima as a function of Pb(II) concentration in the range of  $2.5 \times 10^{-7}$ – $5.0 \times 10^{-5}$  mol/L (c) and  $2.5 \times 10^{-7}$ – $1.0 \times 10^{-5}$  mol/L (d)

with the transition of lone pair electrons to naphthalimide is inhibited, resulting in the enhanced fluorescent responsiveness. Among the divalent metal ions, Pb(II) is special. Figure 8 shows the hypothetical complexation model between FCNCs and Pb(II). The impressive fluorescent responsiveness of FCNCs to Pb(II) can be attributed to the strong complexation between Pb(II) and FCNCs, which greatly affects the ICT process. While other divalent ions including Ba(II), Cu(II), Zn(II), Fe(II), Co(II), Ni(II), and Mg(II), may have relatively weak chelation with FCNCs and hence lead to slight fluorescence enhancement.

To further study the sensing mechanism of FCNCs to Pb(II), Job's plot experiment was carried out and the fluorescence maxima versus the mole fraction of Pb(II) was measured. As shown in Fig. 9, the fluorescence maxima is achieved when the molar fraction of Pb(II) is 0.55, indicating that a 1.2:1 complex is formed between Pb(II) and ANI groups of FCNCs in aqueous solution. It is basically consistent with the theoretically predicted complex ratio of 1:1 illustrated in Fig. 8. Since there are more carboxyl groups than dye groups on the surface of FCNCs, the direct combination of Pb(II) with carboxyl in the absence of dye groups may lead to the small increase in the measured complex ratio.

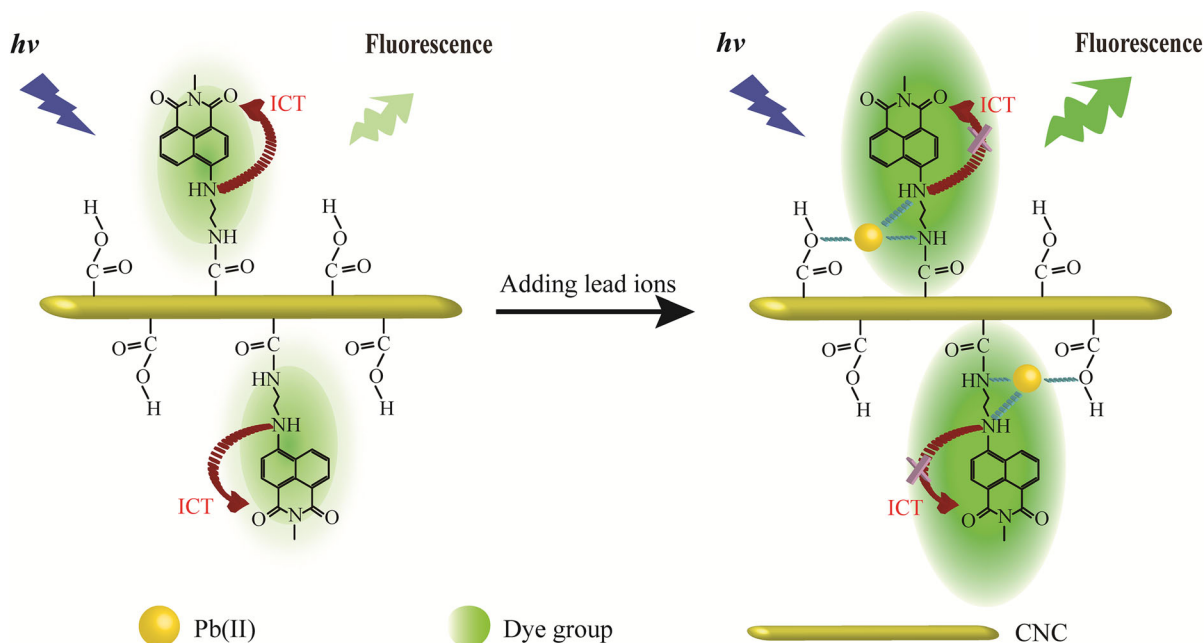


**Fig. 8** Complexation model between Pb(II) and FCNCs

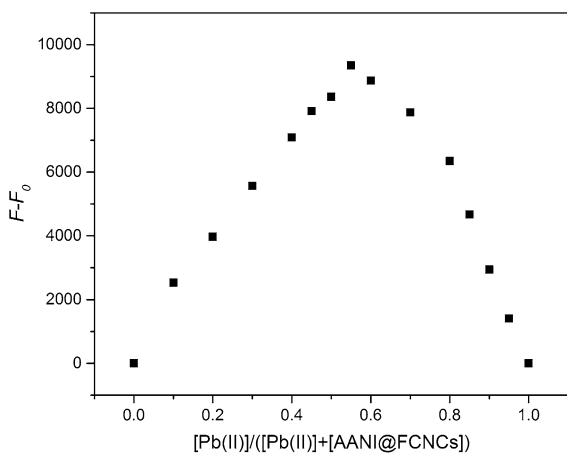


**Fig. 9** Job's plot for FCNCs versus Pb(II), total concentration ( $[\text{Pb(II)}] + [\text{AANI@FCNCs}]$ ):  $5.0 \times 10^{-5}$  mol/L, AANI@FCNCs: the fluorophore immobilized on FCNCs,  $F$  and  $F_0$ : the maximal fluorescent intensity with and without Pb(II), respectively

## Conclusions

A water-dispersible fluorescent probe based on CNCs for the sensitive and selective detection of Pb(II) was fabricated via covalently combining 1,8-naphthalimide with CNC substrate. The CNC probe shows an

exclusively selective fluorescent response to Pb(II) among 11 metal ions in aqueous solution compared with pure 1,8-naphthalimide dye. The fluorescence enhancement factor is high up to 9.5, and the detection performance is little affected in the presence of co-existing metal ions. The LOD of Pb(II) is determined to be  $1.5 \times 10^{-7}$  mol/L and there is good linear relationship between the maximum fluorescent intensity and the Pb(II) concentration in the range of  $2.5 \times 10^{-7}$ – $5.0 \times 10^{-5}$  mol/L. The fluorophore on FCNCs coordinates with Pb(II) at a stoichiometry of 1:1.2, which is basically consistent with the theoretically predicted complex ratio of 1:1. The new type of fluorescent probe will provide not only practical methods for the detection of Pb(II) in aqueous solutions but also application to biological imaging and other aspects owing to the harmless nano-substrate and responsive fluorescence emission.

**Acknowledgments** The support of this work by Natural Science Foundation of Jiangsu Province (BK20171450), National Natural Science Foundation of China (61571239), and the Foundation of State Key Laboratory of Biobased Material and Green Papermaking (Nos. KF201804, QiluUniversity of Technology, Shandong Academy of Sciences) is gratefully acknowledged.

## Compliance with ethical standards

**Conflict of interest** The authors declare that they have no conflict of interest.

## References

- Amirjani A, Haghshenas DF (2018) Ag nanostructures as the surface plasmon resonance (SPR)-based sensors: a mechanistic study with an emphasis on heavy metallic ions detection. *Sens Actuators B Chem* 273:1768–1779
- Benhamou K, Dufresne A, Magnin A, Mortha G, Kaddami H (2014) Control of size and viscoelastic properties of nanofibrillated cellulose from palm tree by varying the TEMPO-mediated oxidation time. *Carbohydr Polym* 99:74–83
- Bojinov VB, Konstantinova TN (2007) Fluorescent 4-(2,2,6,6-tetramethylpiperidin-4-ylamino)-1,8-naphthalimide pH chemosensor based on photoinduced electron transfer. *Sens Actuators B Chem* 123:869–876
- Chang J, Singh J, Kim S, Hockaday WC, Sim C, Kim SJ (2016) Solid-state NMR reveals differential carbohydrate utilization in diapausing *Culex pipiens*. *Sci Rep* 6:37350
- Chatterjee S, Pramanik S, Hossain SU, Bhattacharya S, Bhattacharya SC (2007) Synthesis and photoinduced intramolecular charge transfer of N-substituted 1,8-naphthalimide derivatives in homogeneous solvents and in presence of reduced glutathione. *J Photochem Photobiol A Chem* 187:64–71
- Chen X, Pradhan T, Wang F, Kim JS, Yoon J (2011) Fluorescent chemosensors based on spiroring-opening of xanthenes and related derivatives. *Chem Rev* 112:1910–1956
- Chen J, Zhou Z, Chen Z, Yuan W, Li M (2017) A fluorescent nanoprobe based on cellulose nanocrystals with porphyrin pendants for selective quantitative trace detection of  $Hg^{2+}$ . *New J Chem* 41:10272–10280
- Chen W, Zhang S, Dai G, Chen Y, Li M, Zhao X, Chen Y, Chen L (2019) Tuning the photophysical properties of symmetric squarylium dyes: investigation on the halogen modulation effects. *Chem Eur J* 25:469–473
- Ding Q, Zeng J, Wang B, Gao W, Chen K, Yuan Z, Xu J (2017) Influence of binding mechanism on labeling efficiency and luminous properties of fluorescent cellulose nanocrystals. *Carbohydr Polym* 175:105–112
- Duke RM, Veale EB, Pfeffer FM, Kruger PE, Gunnlaugsson T (2010) Colorimetric and fluorescent anion sensors: an overview of recent developments in the use of 1,8-naphthalimide-based chemosensors. *Chem Soc Rev* 39:3936–3953
- Eisa WH, Abdelgawad AM, Rojas OJ (2018) Solid-state synthesis of metal nanoparticles supported on cellulose nanocrystals and their catalytic activity. *ACS Sustain Chem Eng* 6:3974–3983
- Fu Y, Yu W, Zhang W, Huang Q, Yan J, Pan C, Yu G (2018) Sulfur-rich covalent triazine polymer nanospheres for environmental mercury removal and detection. *Polym Chem* 9:4125–4131
- Fukuzumi H, Saito T, Isogai A (2013) Influence of TEMPO-oxidized cellulose nanofibril length on film properties. *Carbohydr Polym* 93:172–177
- Ghassemi Z, Slaughter G (2018) Storage stability of electrospun pure gelatin stabilized with EDC/Sulfo-NHS. *Biopolymers* 109:e23232
- Golmohammadi H, Morales-Narvaez E, Naghdi T, Merkoci A (2017) Nanocellulose in sensing and biosensing. *Chem Mater* 29:5426–5446
- Grabtchev I, Konstantinov T, Guittonneau S, Meallier P (1997) Photochemistry of some 1,8-naphthalic anhydride derivatives. *Dyes Pigments* 35:361–366
- Jiang W, Yang S, Lu W, Gao B, Xu L, Sun X, Jiang D, Xu H-J, Ma M, Cao F (2018) A novel fluorescence “turn off-on” nano-sensor for detecting  $Cu^{2+}$  and Cysteine in living cells. *J Photochem Photobiol A Chem* 362:14–20
- John H (1990) The UV-visible absorption and fluorescence of some substituted 1,8-naphthalimides and naphthalic anhydrides. *J Chem Soc Perkin Trans* 2:837–842
- Liu J, Ren X, Meng X, Fang Z, Tang F (2013) Sensitive and selective detection of  $Hg^{2+}$  and  $Cu^{2+}$  ions by fluorescent Ag nanoclusters synthesized via a hydrothermal method. *Nanoscale* 5:10022–10028
- Loving G, Imperiali B (2009) Thiol-reactive derivatives of the solvatochromic 4-N,N-dimethylamino-1,8-naphthalimide fluorophore: a highly sensitive toolset for the detection of biomolecular interactions. *Bioconj Chem* 20:2133–2141
- Makwana BA, Vyas DJ, Bhatt KD, Jain VK, Agrawal YK (2015) Highly stable antibacterial silver nanoparticles as selective fluorescent sensor for  $Fe^{3+}$  ions. *Spectrochim Acta Part A* 134:73–80
- Martin E, Weigand R, Pardo A (1996) Solvent dependence of the inhibition of intramolecular charge-transfer in N-substituted 1,8-naphthalimide derivatives as dye lasers. *J Lumin* 68:157–164
- Nandhikonda P, Paudel S, Heagy MD (2009) Minimal modification approach to red-shifted absorption and fluorescence in 1,8-naphthalimides. *Tetrahedron* 65:2173–2177
- Navarro JR, Conzatti G, Yu Y, Fall AB, Mathew R, Edén M, Bergström L (2015) Multicolor fluorescent labeling of cellulose nanofibrils by click chemistry. *Biomacromol* 16:1293–1300
- Neupane LN, Oh E-T, Park HJ, Lee K-H (2016) Selective and sensitive detection of heavy metal ions in 100% aqueous solution and cells with a fluorescence chemosensor based on peptide using aggregation-induced emission. *Anal Chem* 88:3333–3340
- Powell HM, Boyce ST (2006) EDC cross-linking improves skin substitute strength and stability. *Biomaterials* 27:5821–5827
- Rasheed T, Li C, Nabeel F, Huang W, Zhou Y (2019) Self-assembly of alternating copolymer vesicles for the highly selective, sensitive and visual detection and quantification of aqueous  $Hg^{2+}$ . *Chem Eng J* 358:101–109
- Salarvand Z, Amirnasr M, Meghdadi S (2019) Colorimetric and fluorescent sensing of  $Al^{3+}$  by a new 2-hydroxynaphthalen based Schiff base “off-on” chemosensor. *J Lumin* 207:78–84
- Sam S, Touahir L, Salvador Andresa J, Allongue P, Chazalviel J-N, Gouget-Laemmel A, Henry de Villeneuve C, Moraillon A, Ozanam F, Gabouze N (2009)

- Semiquantitative study of the EDC/NHS activation of acid terminal groups at modified porous silicon surfaces. *Langmuir* 26:809–814
- Shaki H, Gharanjig K, Rouhani S, Khosravi A (2010) Synthesis and photophysical properties of some novel fluorescent dyes based on naphthalimide derivatives. *J Photochem Photobiol A* 216:44–50
- Slama-Schwok A, Blanchard-Desce M, Lehn J (1990) Intramolecular charge transfer in donor–acceptor molecules. *J Phys Chem* 94:3894–3902
- Suárez PL, García-Cortés M, Fernández-Argüelles MT, Encinar JR, Valledor M, Ferrero FJ, Campo JC, Costa-Fernández JM (2018) Functionalized phosphorescent nanoparticles in (bio) chemical sensing and imaging—a review. *Anal Chim Acta* 1046:16–31
- Tang L, Li T, Zhuang S, Lu Q, Li P, Huang B (2016) Synthesis of pH-sensitive fluorescein grafted cellulose nanocrystals with an amino acid spacer. *ACS Sustain Chem Eng* 4:4842–4849
- Wang S, Sun J, Gao F (2015) A turn-on near-infrared fluorescent chemosensor for selective detection of lead ions based on a fluorophore–gold nanoparticle assembly. *Analyst* 140:4001–4006
- Wang P, Yao K, Fu J, Chang Y, Li B, Xu K (2019) Novel fluorescent probes for relay detection copper/citrate ion and application in cell imaging. *Spectrochim Acta A* 211:9–17
- Ward CC, Kleinman JI, Nomura DK (2017) NHS-esters as versatile reactivity-based probes for mapping proteome-wide ligandable hotspots. *ACS Chem Biol* 12:1478–1483
- Wu W, Huang F, Pan S, Mu W, Meng X, Yang H, Xu Z, Ragauskas AJ, Deng Y (2015) Thermo-responsive and fluorescent cellulose nanocrystals grafted with polymer brushes. *J Mater Chem* 3:1995–2005
- Wu H, Jia J, Xu Y, Qian X, Zhu W (2018a) A reusable bifunctional fluorescent sensor for the detection and removal of silver ions in aqueous solutions. *Sens Actuators B Chem* 265:59–66
- Wu W, Song R, Xu Z, Jing Y, Dai H, Fang G (2018b) Fluorescent cellulose nanocrystals with responsiveness to solvent polarity and ionic strength. *Sens Actuators B Chem* 275:490–498
- Xia B, Wang B, Shi J, Zhang W, Xiao S (2014) Engineering near-infrared fluorescent styrene-terminated porous silicon nanocomposites with bovine serum albumin encapsulation for in vivo imaging. *J Mater Chem B* 2(47):8314–8320
- Xie J, Jiang X, Zhong Y, Lu Y, Wang S, Wei X, Su Y, He Y (2014) Stem-loop DNA-assisted silicon nanowires-based biochemical sensors with ultra-high sensitivity, specificity, and multiplexing capability. *Nanoscale* 6:9215–9222
- Zhang J, Yu S-H (2014) Highly photoluminescent silicon nanocrystals for rapid, label-free and recyclable detection of mercuric ions. *Nanoscale* 6:4096–4101
- Zhang L, Li Q, Zhou J, Zhang L (2012) Synthesis and photophysical behavior of pyrene-bearing cellulose nanocrystals for Fe<sup>3+</sup> sensing. *Macromol Chem Phys* 213:1612–1617
- Zhang YJ, Ma XZ, Gan L, Xia T, Shen J, Huang J (2018) Fabrication of fluorescent cellulose nanocrystal via controllable chemical modification towards selective and quantitative detection of Cu(II) ion. *Cellulose* 25:5831–5842
- Zhao L, Li W, Plog A, Xu Y, Buntkowsky G, Gutmann T, Zhang K (2014) Multi-responsive cellulose nanocrystal–rhodamine conjugates: an advanced structure study by solid-state dynamic nuclear polarization (DNP) NMR. *Phys Chem Chem Phys* 16:26322–26329
- Zhou J, Butchosa N, Jayawardena HSN, Park J, Zhou Q, Yan MD, Ramstrom O (2015) Synthesis of multifunctional cellulose nanocrystals for lectin recognition and bacterial imaging. *Biomacromolecules* 16:1426–1432

**Publisher's Note** Springer Nature remains neutral with regard to jurisdictional claims in published maps and institutional affiliations.